Accepted Manuscript

Title: Cell adhesion and spreading at a charged interface: Insight into the mechanism using surface techniques and mathematical modelling

Author: Nadica Ivošević DeNardis Jadranka Pečar Ilić Ivica Ružić Galja Pletikapić
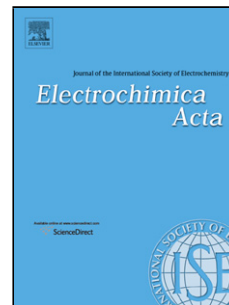
Please cite this article as: Nadica Ivošević DeNardis, Jadranka Pečar Ilić, Ivica Ružić, Galja Pletikapić, Cell adhesion and spreading at a charged interface: Insight into the mechanism using surface techniques and mathematical modelling, Electrochimica Acta http://dx.doi.org/10.1016/j.electacta.2015.07.068

Cell adhesion and spreading at a charged interface: Insight into the mechanism using surface techniques and mathematical modelling

Nadica Ivošević DeNardis*[1], Jadranka Pečar Ilić, Ivica Ružić, Galja Pletikapić

Division for Marine and Environmental Research, Ruđer Bošković Institute, POB 180, HR-10002 Zagreb, Croatia

*Corresponding author:

Tel: +385 1 4561-128

Fax: +385 1 4680-242

E-mail address: ivosevic@irb.hr (N. Ivošević DeNardis)

---

[1] ISE member

Highlights

- Kinetics of adhesion and spreading of the algal cell at a charged interface is explored.

- Amperometric signals are analyzed using extended methodology and the reaction kinetics model.

- The model reconstructs and quantifies individual states of the three-step adhesion process.

- Adhesion kinetics of the algal cell is slower than that of its plasma membrane vesicle.

- Slow spreading of organic film at the interface could be due to the attenuated effect of the potential.

Abstract

We study the kinetics of adhesion and spreading of an algal cell and its plasma membrane vesicle at the charged interface. A simple system of an isolated plasma membrane vesicle without internal content has been developed and characterized by atomic force microscopy (AFM). We extend the methodology based on the reaction kinetics model and empirical fitting for the analysis of amperometric signals, and demonstrate its validity and pertinence in a wide range of surface charge densities. Adhesion kinetics of the algal cell is slower than that of its plasma membrane vesicle. Isolated plasma membrane contributes about one quarter to the cell contact area. The model reconstructs and quantifies individual states of the three-step adhesion process of the algal cell and makes it possible to associate them with various features of amperometric signal. At the

time of current amplitude, the ruptured state predominates and the cell contact area is larger than its initial area as well as the contact area of the plasma membrane vesicle. These results suggest that a major structural disruption of the cell membrane, collapse of cytoskeleton and leakage of intracellular material could appear close to the time of current amplitude. Further, kinetics of the organic film spreading at the interface to its maximal extent is considered as the rate determining step, which could be a consequence of the attenuated effect of potential at the modified interface, stronger intermolecular interactions and reorganization of molecules in the film. Our findings offer an insight into the mechanism of algal cell adhesion and spreading at charged interfaces, relevant for electroporation based studies.

Keywords: amperometry, cell adhesion, charged interface, kinetics, mathematical model

1. INTRODUCTION

Interfacial behaviour of supported lipid layers, vesicles, model membranes and cells has been extensively studied at the mercury interface [1-15]. Techniques employing a mercury electrode are essential for membrane studies, due to the unique advantage of mercury as a fluid and conductive surface. Recently, an important step forward has been made by integrating a renewable mercury electrode into an AFM setup, opening new perspectives to simultaneous coupling of the membrane mechanics with its electrochemical or electrical properties [16]. The single cell-electrode interaction is relevant to fundamental biological processes involving cell adhesion, cell fusion, cell activity, and membrane response to

environmental stress. We previously studied adhesion of the algal cell *Dunaliella tertiolecta* (*D. tertiolecta*) to the charged interface by recording the amperometric signal. The signal denotes establishment of intimate membrane contact at the charged mercury interface with subsequent cell spreading, followed by cell breakdown in a few milliseconds [10,11]. Analogously, the Scholz group studied adhesion of thrombocyte vesicles and mitochondria to the static mercury electrode [17,18]. They reported that the adhesion-spreading behaviour of a thrombocyte vesicle exhibits similarity with the *D. tertiolecta* algal cell. The integrated current transient of the thrombocyte vesicle was fitted with the empirical equation of the three-step process in order to access the kinetic parameters of adhesion-spreading processes. They found that the model yielded unrealistic best-fit parameters due to their large average errors. Independently, based on the reaction scheme, we developed a mathematical model for the kinetics of the adhesion event based on consecutive two- and three-step processes of the first-order with analytical solutions of the individual components of the process. Corresponding methodology based on the model makes it possible to distinguish between the two- and three-step processes and to extract kinetic parameters of the adhesion process [19,20]. Recently, the reaction kinetics model was tested and validated on amperometric signals of empty phospholipid vesicles, showing that all of the three distinct states simultaneously evolve from the onset of the two-step adhesion process [21]. Mechanical model showing that the rate of transformation of the liposome cap volume into the skirt is controlled by flux through pores implies that the release of liposome content across the cap membrane through many transient pores is a realistic scenario, indirectly supported by the exceedingly large hydraulic conductivity of the membrane [21]. To the best of our knowledge, kinetics of *D. tertiolecta* cell adhesion has not been studied so far and presents a challenge, since algal cells are motile charged particles possessing a complex photosynthetic machinery. The unicellular green flagellate *Dunaliella* is the most widely studied member of Chlorophyceae. Unique to

Dunaliella is the absence of a rigid cell wall possessing a glycocalyx type cell envelope [22]. It appears in habitats with a wide range of salinity, pH, light intensity and temperature. Due to these features, interest in fundamental and biochemical research of *Dunaliella* has been increasing. *Dunaliella* has been studied as a model for osmoregulation, pigment production, and for commercial mass cultures [23]. *D. tertiolecta* cell suspension in 0.1 M aqueous electrolyte solution is a suitable system for electrochemical detection, serving as a standard for calibration of adhesion responses of surface-active particles in aquatic systems [9,24]. The aim here is to study the kinetics of adhesion and spreading of more complex systems such as algal cells at a charged interface. In order to better understand the mechanism of algal cell adhesion, a simple system of isolated cell envelope without internal content has been developed and characterized accordingly. For the first time, we apply and test the reaction kinetics model in order to show how the distinct states of an adhesion event can be associated with various features of the amperometric signal of the algal cell. We validate the methodology based on the reaction kinetics model on amperometric signals recorded in a wide potential range.

2. EXPERIMENTAL

2.1. Cell suspensions

We used a laboratory culture of the unicellular marine algae *Dunaliella tertiolecta* Butcher (Chlorophyceae). The cells (maximum dimension 6-12 μm) were grown in seawater enriched with F-2 medium [25] in a batch culture under ambient conditions. Cell density in the culture reached up to 2×10^6 cells/mL after 14 days of growth. The cells were separated from the growth medium by mild centrifugation (1500 g, 5 min). The

loose pellet was washed several times with filtered seawater. Stock suspension contained $1\text{-}6\times10^7$ cells/mL. Diluted suspensions submitted to electrochemical measurements were controlled by light microscopy in terms of cell density and viability.

2.2. Isolation of cell envelope (plasma membrane vesicle)

The loose algal cell pellet was diluted 40 times with ultrapure water. Tubes were first vigorously shaken on a vortex and then left at room temperature. After 30 minutes, most of the cells had completely or partially released intracellular material due to the osmotic shock. The suspension was centrifuged at 1500 g for 5 min. The pellet containing cell debris and not completely empty plasma membrane vesicles was removed and the supernatant was centrifuged at 15 000 g for 15 min. The new supernatant was further centrifuged at 45 000 g for 15 min. The pellet containing empty plasma membrane vesicles in a size range of several µm up to 40 µm was resuspended in 3 mL of ultrapure water (~10^4 vesicle/mL).

2.3. Atomic force microscopy (AFM)

AFM connects the nanometer and micrometer length scales utilizing a sharp probe tip that senses interatomic forces acting between the surface of a sample and the atoms at the apex of the tip. The physical basis behind AFM and its ability to "feel" the surface make AFM a versatile tool in

biophysics, allowing high resolution imaging, nanomechanical characterization and measurements of inter and intramolecular forces in living and non-living structures. Its use includes an electronic control unit, computer and usually two monitors for simultaneous checking of the image and imaging parameters. The probe which scans the sample surface consists of a cantilever and the tip located at the free end of the cantilever. The deflection of the cantilever is measured by an optical detection system. Registered values of cantilever deflection are electronically converted into a pseudo 3D image of a sample. AFM is a non-destructive method that gives real 3D images of the sample with a vertical resolution of 0.1 nm and lateral resolution of 1 nm. Measured forces range from 10^{-6} N to 10^{-11} N.

2.4. Sample preparation for AFM imaging and AFM measurements

For AFM imaging, a 5 µL volume of the suspension containing plasma membrane vesicles was pipetted directly onto freshly cleaved mica and allowed to dry for 30 min in an enclosed Petri dish before imaging. AFM imaging of plasma membrane vesicles was performed using a MultiMode Scanning Probe Microscope with a Nanoscope IIIa controller (Bruker, Billerica USA) with a vertical engagement (JV) 125 µm scanner. Images were recorded in contact mode using a standard silicon nitride tip (NP-20, Bruker, nominal frequency 56 kHz, nominal spring constant of 0.32 N m^{-1}) with scan resolution of 512 samples per line. Scanning rates were normally optimized around 1-2 Hz. Processing and analysis of images were carried out using the NanoScope^{TM} software (Digital Instruments, Version V614r1 and V531r1). The force was kept at the lowest possible value in order to minimize the forces of interaction between the tip and the surface. Measurements were performed in air, at

room temperature and 50-60 % relative humidity, which leaves the samples with a small hydration layer, helping to maintain the structure [26] using freshly cleaved mica as a substrate. All images are presented as raw data except for the first-order two-dimensional flattening.

2.5. Electrochemical measurements

Dropping mercury electrode (DME) had a drop-life of 2.0 seconds, flow rate of 6.0 mg/s and a maximum surface area of 4.57 mm^2. All potentials were referred to an Ag/AgCl (0.1 M NaCl) reference electrode, which was separated from the measured dispersion by a ceramic frit. Electrochemical experiments were performed in a standard Methrom vessel with a 20 mL volume of cell suspension at 25 $^{\circ}$C. An aliquot of stock cell suspension was added directly into the deaerated solution, prior to electrochemical measurement. The aqueous solution contained 0.1 M NaCl and 5 mM NaHCO$_3$ to maintain pH at 8.2. Electrochemical measurements were performed using a PAR 174A Polarographic Analyzer interfaced to a computer. The potentiostat PAR 174A had two main parts: the voltage source and the measuring circuit. It was found that the measuring circuit was the slowest part, and its rise time was measured by applying a signal with negligible rise time to its input, with the selector set to dummy cell mode. The rise time of the measuring circuit determined for different current ranges had a value of 0.1 ms. Thus the time constant of PAR 174A was 0.045 ms. Acquisition of analog signals was performed with a DAQ card-AI-16-XE-50 (National Instruments) input device and the data were analyzed using an application developed in the *LabView* 6.1 software package. The current-time (*I-t*) curves over 50 mercury drop lives were recorded at constant potentials with temporal resolution of 20 μs. The measured signal has a specific waveform

represented as the difference between two exponential functions of time. Approximating the measuring signal with a linear or an exponential function is the preferred way to analyze such a waveform: in this case, the influence of the time constant of the potentiostat is much smaller than for the step function. Such an approximation introduces a delay and a slight change in amplitude of the output signal but it enables measurement of the time constants of the process even if they are comparable to the time constant of the potentiostat.

2.6. Electrochemical method

Adhesion and spreading of organic particles at a charged mercury/water interface cause double-layer charge displacement from the inner Helmholtz plane, and the transient flow of compensating current can be recorded as an amperometric signal. Each amperometric signal corresponds to the adhesion of a single particle from suspension [9,12]. Random occurrence of the adhesion events is due to the spatial heterogeneity inherent to a dispersed system and to the stochastic nature of the particles' encounter with the electrode. At a given potential, the current amplitude reflects the size of the adhered particle while the signal frequency reflects the particle concentration in the suspension [9,10,24,27]. The lower size-detection limit is ≥ 3 µm under deaerated conditions. Signals are defined by their amplitude (i.e. peak of adhesion signal) I_m and duration t_d as well as by displaced charge q_D [10,11,27]. The displaced double-layer charge is obtained by integrating the area under the signal:

$$q_{\mathrm{D}} = \int_{t_i}^{t_i+t_d} I \mathrm{d}t \qquad (1)$$

If charge displacement is complete, which leads to the formation of an organic layer, the area of the contact interface A_c is determined from the amount of displaced charge:

$$A_c = \frac{q_{\mathrm{D}}}{\sigma_{12}} \qquad (2)$$

where σ_{12} is the surface charge density of the mercury/aqueous electrolyte.

According to the modified Young-Dupré equation, the total Gibbs energy of interaction between an organic droplet and the aqueous mercury interface is

$$-\Delta G = A(\gamma_{12} - \gamma_{23} - \gamma_{13}) \qquad (3)$$

where γ_{12}, γ_{13} and γ_{23} are the interfacial energies at mercury/water, mercury/organic liquid and water/organic liquid interfaces, respectively.

The expression in parentheses is the spreading coefficient (S_{132}) at the three-phase boundary [28]. When $S_{132} > 0$, attachment and spreading are spontaneous processes, while when $S_{132} < 0$, spreading is not spontaneous. The critical interfacial tension of adhesion $(\gamma_{12})_c$ defined by $S_{132} = 0$ will be $(\gamma_{12})_c = \gamma_{13} + \gamma_{23}$.

3. THEORY

The kinetics of organic particle adhesion to a charged interface can be described as a process involving three steps. The three-step adhesion process is illustrated by four states: initial intact state (A), two intermediate states (B, C), which could be associated with deformation and rupture, and the final state of product formation (D). The three-step process is represented by the following reaction scheme:

$$A \xrightleftharpoons[k_2]{k_1} B \xrightleftharpoons[k_4]{k_3} C \xrightleftharpoons[k_6]{k_5} D \qquad (4)$$

This reaction scheme involves four states of the organic particle in contact with the charged interface, where k_1, k_3, and k_5 are the forward rate constants, while k_2, k_4 and k_6 are the backward rate constants. The reaction scheme is represented by a set of four differential equations in terms of the rate constants [20]:

$$\frac{\mathrm{d}A}{\mathrm{d}t} = -k_1 A + k_2 B \qquad (5)$$

$$\frac{\mathrm{d}B}{\mathrm{d}t} = k_1 A - (k_2 + k_3)B + k_4 C \qquad (6)$$

$$\frac{\mathrm{d}C}{\mathrm{d}t} = k_3 B - (k_4 + k_5)C + k_6 D \qquad (7)$$

$$\frac{\mathrm{d}D}{\mathrm{d}t} = k_5 C - k_6 D \qquad (8)$$

with initial conditions: at $t = 0$, $A = A_0$, $B = C = D = 0$, and the corresponding continuity relation $A + B + C + D = A_0$. Here, we apply Laplace transforms to convert the system of linear differential equations (5)-(8) into the corresponding algebraic equations, in order to efficiently obtain solutions for each individual state. Laplace transform $\mathcal{L}[f(t)]$ translates the function of a real variable $f(t)$ into the corresponding function of a complex variable $F(s)$. After the corresponding solution is derived in the Laplace domain, using the inverse Laplace transform $\mathcal{L}^{-1}[F(s)] = f(t)$ yields this solution back in the real (time) domain. Therefore, solutions for individual states A, B, C and D in the Laplace domain are obtained as follows:

$$\mathcal{L}[A(t)] = \frac{A_0}{s + k_1}\left(1 + \frac{k_1 k_2}{\delta}\left(s^2 + s(k_4 + k_5 + k_6) + k_4 k_6\right)\right) \tag{9}$$

$$\mathcal{L}[B(t)] = \frac{A_0 k_1}{\delta}\left(s^2 + s(k_4 + k_5 + k_6) + k_4 k_6\right) \tag{10}$$

$$\mathcal{L}[C(t)] = \frac{A_0 k_1 k_3}{\delta}\left(s + k_6\right) \tag{11}$$

$$\mathcal{L}[D(t)] = \frac{A_0 k_1 k_3 k_5}{\delta} \tag{12}$$

where function δ defines the contribution of individual states in terms of the rate constants and reads:

$$\delta = s\left\{s^3 + s^2\left(k_1 + k_2 + k_3 + k_4 + k_5 + k_6\right) + s\left[\left(k_1 + k_2 + k_3\right)\left(k_4 + k_5 + k_6\right) + \right.\right.$$
$$\left.\left. + k_1 k_3 + k_4 k_6 - k_3 k_4\right] + k_4 k_6\left(k_1 + k_2\right) + k_1 k_3\left(k_5 + k_6\right)\right\} \tag{13}$$

The relation between rate and time constants is established using the following system of three algebraic equations (equivalent to a cubic equation):

$$1/\tau_0 + 1/\tau_1 + 1/\tau_2 = k_1 + k_2 + k_3 + k_4 + k_5 + k_6 \tag{14}$$

$$1/\tau_0\tau_1 + 1/\tau_0\tau_2 + 1/\tau_1\tau_2 = (k_1 + k_2 + k_3)(k_4 + k_5 + k_6) + k_1 k_3 + k_4 k_6 - k_3 k_4 \tag{15}$$

$$1/\tau_0\tau_1\tau_2 = k_4 k_6 (k_1 + k_2) + k_1 k_3 (k_5 + k_6) \tag{16}$$

Accordingly, function δ can be rearranged in terms of separated components with the corresponding time constants τ_0, τ_1, τ_2 and constants α, β and γ as follows:

$$\frac{1}{\delta} = \frac{1}{s(s + 1/\tau_0)(s + 1/\tau_1)(s + 1/\tau_2)} = \frac{\alpha}{s(s + 1/\tau_0)} + \frac{\beta}{s(s + 1/\tau_1)} + \frac{\gamma}{s(s + 1/\tau_2)} \tag{17}$$

Further, solutions for the individual states (A, B, C and D) in the time domain can be derived, applying the inverse Laplace trasformations for Equations (9)-(12) previously rearranged by introducing Eq. (17). The initial state A obtained according to Eq. (9) reads:

$$A = A_\infty - A_\infty \left[\left(\tau_0^2 - \frac{\tau_0(k_3 + k_4 + k_5 + k_6) - 1}{k_4 k_6 + k_3 k_5 + k_3 k_6} \right) \frac{\exp\left(-\dfrac{t}{\tau_0}\right)}{(\tau_1 - \tau_0)(\tau_2 - \tau_0)} - \left(\tau_1^2 - \frac{\tau_1(k_3 + k_4 + k_5 + k_6) - 1}{k_4 k_6 + k_3 k_5 + k_3 k_6} \right) \right.$$

$$\left. \frac{\exp\left(-\dfrac{t}{\tau_1}\right)}{(\tau_1 - \tau_0)(\tau_2 - \tau_1)} + \left(\tau_2^2 - \frac{\tau_2(k_3 + k_4 + k_5 + k_6) - 1}{k_4 k_6 + k_3 k_5 + k_3 k_6} \right) \frac{\exp\left(-\dfrac{t}{\tau_2}\right)}{(\tau_2 - \tau_0)(\tau_2 - \tau_1)} \right] \qquad (18)$$

where $A_\infty = k_2 k_4 k_6 \tau_0 \tau_1 \tau_2 A_0$ represents the equilibrium value of the initial state. The first intermediate state B is obtained from Eq. (10):

$$B = B_\infty - B_\infty \left[\left(\tau_0^2 - \frac{\tau_0(k_4 + k_5 + k_6) - 1}{k_4 k_6} \right) \frac{\exp\left(-\dfrac{t}{\tau_0}\right)}{(\tau_1 - \tau_0)(\tau_2 - \tau_0)} - \left(\tau_1^2 - \frac{\tau_1(k_4 + k_5 + k_6) - 1}{k_4 k_6} \right) \right.$$

$$\left. \frac{\exp\left(-\dfrac{t}{\tau_1}\right)}{(\tau_1 - \tau_0)(\tau_2 - \tau_1)} + \left(\tau_2^2 - \frac{\tau_2(k_4 + k_5 + k_6) - 1}{k_4 k_6} \right) \frac{\exp\left(-\dfrac{t}{\tau_2}\right)}{(\tau_2 - \tau_0)(\tau_2 - \tau_1)} \right] \qquad (19)$$

where $B_\infty = k_1 k_4 k_6 \tau_0 \tau_1 \tau_2 A_0$ represents the corresponding equilibrium value. The second intermediate state C is obtained from Eq. (11):

$$C = C_\infty - C_\infty \left[\frac{\left(\tau_0^2 - \frac{1}{k_6} \right) \exp\left(-\frac{t}{\tau_0} \right)}{\left(\tau_1 - \tau_0 \right)\left(\tau_2 - \tau_0 \right)} - \frac{\left(\tau_1^2 - \frac{1}{k_6} \right) \exp\left(-\frac{t}{\tau_1} \right)}{\left(\tau_1 - \tau_0 \right)\left(\tau_2 - \tau_1 \right)} + \frac{\left(\tau_2^2 - \frac{1}{k_6} \right) \exp\left(-\frac{t}{\tau_2} \right)}{\left(\tau_2 - \tau_0 \right)\left(\tau_2 - \tau_1 \right)} \right] \qquad (20)$$

where $C_\infty = k_1 k_3 k_6 \tau_0 \tau_1 \tau_2 A_0$ represents the equilibrium value of the second intermediate. The final state D is obtained according to Eq. (12) and

reads [20]:

$$D = D_0 \left[1 - \exp\left(-\frac{t}{\tau_0} \right) \right] - D_1 \left[1 - \exp\left(-\frac{t}{\tau_1} \right) \right] + D_2 \left[1 - \exp\left(-\frac{t}{\tau_2} \right) \right]$$

$$= D_\infty - D_\infty \left[\frac{\tau_0^2 \exp\left(-\frac{t}{\tau_0} \right)}{\left(\tau_1 - \tau_0 \right)\left(\tau_2 - \tau_0 \right)} - \frac{\tau_1^2 \exp\left(-\frac{t}{\tau_1} \right)}{\left(\tau_1 - \tau_0 \right)\left(\tau_2 - \tau_1 \right)} + \frac{\tau_2^2 \exp\left(-\frac{t}{\tau_2} \right)}{\left(\tau_2 - \tau_0 \right)\left(\tau_2 - \tau_1 \right)} \right] \qquad (21)$$

where D_0, D_1 and D_2 are the corresponding pre-exponential constants and $D_\infty = k_1 k_3 k_5 \tau_0 \tau_1 \tau_2 A_0$ represents the equilibrium value of the final

state. The same solution can be obtained from the continuity realation $D = A_0 - A - B - C$. The analytical solutions of the reaction kinetics

model provide a basis for the determination of time dependence of the four different states that coexist simultaneously during the three-step

process, according to Eqs. (18)-(21), respectively.

In order to obtain the time dependence of states A and B in the irreversible variant of the process, the conditions $A_\infty = B_\infty = 0$, $k_1 = 1/\tau_0$ and $k_3 = 1/\tau_1$ are introduced into Eqs. (18) and (19). In this case,

$$A = A_0 \exp\left(-\frac{t}{\tau_0}\right) \tag{22}$$

and

$$B = \frac{\tau_1 A_0}{\tau_1 - \tau_0}\left[\exp\left(-\frac{t}{\tau_1}\right) - \exp\left(-\frac{t}{\tau_0}\right)\right]. \tag{23}$$

For the time dependence of state C, the conditions $C_\infty = 0$ and $k_5 = 1/\tau_2$ are introduced into Eq. (20) and it follows:

$$C = \tau_2 A_0 \left[\frac{\tau_0 \exp\left(-\dfrac{t}{\tau_0}\right)}{(\tau_1 - \tau_0)(\tau_2 - \tau_0)} - \frac{\tau_1 \exp\left(-\dfrac{t}{\tau_1}\right)}{(\tau_1 - \tau_0)(\tau_2 - \tau_1)} + \frac{\tau_2 \exp\left(-\dfrac{t}{\tau_2}\right)}{(\tau_2 - \tau_0)(\tau_2 - \tau_1)}\right] \tag{24}$$

Finally, the time dependence of the final state D is given by Eq. (21), assuming that $D_\infty = A_0$. In order to be applied for the analysis of amperometric measurements, Eq. (21) should be transformed to its electrical equivalent, where the amount of product D and the rate of product formation dD/dt correspond to charge Q and to current I, respectively [20]. Thus,

$$Q(t) = Q_\infty - Q_0 \exp\left(-\frac{t}{\tau_0}\right) + Q_1 \exp\left(-\frac{t}{\tau_1}\right) - Q_2 \exp\left(-\frac{t}{\tau_2}\right)$$

$$= Q_\infty - Q_\infty \left[\frac{\tau_0^2 \exp\left(-\dfrac{t}{\tau_0}\right)}{(\tau_1 - \tau_0)(\tau_2 - \tau_0)} - \frac{\tau_1^2 \exp\left(-\dfrac{t}{\tau_1}\right)}{(\tau_1 - \tau_0)(\tau_2 - \tau_1)} + \frac{\tau_2^2 \exp\left(-\dfrac{t}{\tau_2}\right)}{(\tau_2 - \tau_0)(\tau_2 - \tau_1)} \right] \tag{25}$$

and

$$I(t) = \frac{dQ}{dt} = I_0 \exp\left(-\frac{t}{\tau_0}\right) - I_1 \exp\left(-\frac{t}{\tau_1}\right) + I_2 \exp\left(-\frac{t}{\tau_2}\right)$$

$$= Q_\infty \left[\frac{\tau_0 \exp\left(-\dfrac{t}{\tau_0}\right)}{(\tau_1 - \tau_0)(\tau_2 - \tau_0)} - \frac{\tau_1 \exp\left(-\dfrac{t}{\tau_1}\right)}{(\tau_1 - \tau_0)(\tau_2 - \tau_1)} + \frac{\tau_2 \exp\left(-\dfrac{t}{\tau_2}\right)}{(\tau_2 - \tau_0)(\tau_2 - \tau_1)} \right] \tag{26}$$

where Q_0, Q_1, Q_2, I_0, I_1 and I_2 are the corresponding pre-exponential constants.

According to our methodology [20], four independent kinetic parameters completely define the model of the three-step process. There are three possible selected sets of independent parameters: i) Q_∞, τ_0, τ_1, τ_2; ii) Q_∞, τ_1, τ_2, Q_2 and iii) Q_∞, τ_1, τ_2, I_2 for calculation of dependent parameters. In cases when τ_0 cannot be determined accurately enough from the measured data, the second or third sets of independent parameters should be used. The kinetic parameters τ_0, Q_0 and I_0 could be calculated from the following relation derived from Eq. (26):

$$\frac{\tau_0}{\tau_2}=1-\frac{Q_\infty}{I_2\left(\tau_2-\tau_1\right)}=1-\frac{\tau_2 Q_\infty}{Q_2\left(\tau_2-\tau_1\right)} \tag{27}$$

If the condition $Q_\infty < I_2(\tau_2 - \tau_1)$ is not fulfilled, parameters τ_0, Q_0 and I_0 cannot be obtained (even if high temporal resolution is used for amperometric measurement). Finally, the best fit curve of the three-step process corresponds to the reconstructed current transient using Eq. (26) and the determined kinetic parameters. At very short times $t \to 0$, the initial rising part of the reconstructed current transient reads

$I(t) \to Q_\infty t^2 / 2\tau_0 \tau_1 \tau_2$, so the initial slope increases linearly with time up to the first inflection point. The values of time t_m and current amplitude

I_m are obtained numerically to check the agreement of the best fit curve with amperometric measurements.

4. RESULTS AND DISCUSSION

4.1. Amperometric detection of the D. tertiolecta cell

In general, the algal cell attaches, deforms, ruptures and spreads at the charged interface, causing charge displacement at the distance of the closest approach of about 0.3-0.5 nm [11]. At the selected potential of −400 mV, the electric field is strong (25 MV/m) and the spreading coefficient equals $S_{123} = 22 \,\mathrm{mJ/m^2}$. The application of an electric field to a cell leads to transient permeabilization of the plasma membrane [29]. Fluid membranes rupture if the tensions exceed about 10 mN/m, also known as lysis tension [30]. The membrane breaks when critical density and size of defects are created, leading to a structural change in the membrane, leakage of intracellular content and spreading at the interface. In our experimental setup, visualization of the pores at the cap of the membranes would be rather difficult due to the rapid adhesion process on the millisecond timescale and expanding growth of the mercury surface. Indirect evidence of the rupture of the vesicular membrane was the

exceedingly large hydraulic conductivity of the membrane, found by analyzing the amperometric signal with the mechanical model [21]. The adhesion and spreading of an individual *D. tertiolecta* cell at the charged interface is conveniently studied amperometrically by recording the well defined amperometric signal [10,11]. Fig. 1 shows actual recording of a typical amperometric signal of *D. tertiolecta* cell at the potential of −400 mV (which corresponds to the surface charge density of 3.8 µC/cm^2).

Here Fig. 1.

The signal amplitude has positive direction at a positively charged mercury electrode, i.e. at the potentials of $E > E_{\mathrm{pzc}}$ where E_{pzc} is the point of zero charge. Besides the polarity and the surface charge density of the mercury electrode, the signal amplitude depends on the cell size [11,27]. The signals are characterized by a steep rising portion until the maximum I_{m} is reached at time t_{m}, followed by a slower decay of displacement current, forming the so-called bell-shaped part of the signal. The bell-shaped part of the signal is registered also at the static mercury electrode, so this feature is not contributed by the expanding growth of the mercury surface [31]. The selected signal of the algal cell has current amplitude of 0.72 µA and signal duration is 4.45 ms. The short time scale of adhesion and spreading of cells at the mercury electrode is due to the hydrodynamic regime of the electrode's growing fluid interface [32], enhancing the corresponding process. Our preliminary results (F. Pillet et al. in preparation) show that Young modulus of the cell was low, therefore the effect of cytoskeleton structure on algal cell shape and mechanical properties is not considered to be very large. In the case of *Dunaliella*, the cytoskeleton constitutes an integrated system, in which the basal

bodies and their surrounding material are the central element. It is likely that the submembraneous network of microtubules maintains the

elongated form of this cell. Viscoelastic behaviour of the cell membrane is determined not so much by the cell membrane itself but by the

intracellular cytoskeleton [33].

In signal analysis, the total displaced charge, q_D and contact area, A_c of the interface are calculated using Eqs. (1) and (2). The total displaced

charge is 0.78 nC, which corresponds to the area of the contact interface of 2.05×10^4 μm^2. The amperometric signal captures useful information

about the particle itself and the dynamics of cell adhesion at the interface. The potential range of adhesion of *D. tertiolecta* to the mercury/0.1 M

NaCl interface is from −100 mV to −1150 mV. At a potential more postive and negative than those critical potentials, cells behave as inert

particles. Using electrocapillary data, the experimentally determined critical potential of adhesion corresponds to critical surface charge densities

of 15.6 and −12.4 μC/cm^2 and to critical interfacial tensions of 396 and 383 mJ/m^2 at the positively and negatively charged interface,

respectively. The critical interfacial tension at the negatively charged interface differs from the positively charged interface due to (i) the

contribution of electrostatic repulsion between the negatively charged cell (−0.63 μC/cm^2) and the negatively charged interface [11,31] and (ii)

specific adsorption of chloride ions at the positively charged interface.

4.2. Adhesion kinetics of the D. tertiolecta cell

To analyze the amperometric signal of algal cell, it is essential to accurately determine the initial time and the time when the signal ends, t_d, i.e. when current value decreases below 1 % of current amplitude I_m. The primary part of the signal is characterized by I_{m1}, t_{m1} t_{d1} while the secondary part of the signal is characterized by I_{m2}, t_{m2}, t_{d2} and initial time t_{i2} (when the secondary part appears). We apply the reaction kinetics model of the three-step process and the corresponding methodology (explained in details in Refs. [20,21]) to determine the kinetic parameters of adhesion from the amperometric signal recorded at potential −400 mV (see Fig. 1). The reconstructed current transient is obtained using the determined independent kinetic parameters (τ_0, τ_1, τ_2 and $Q_{\infty 1}$) and Eq. (26). The values of time constants τ_0, τ_1, τ_2 denoting the attachment, deformation and spreading are 0.06 ms, 0.1 ms, and 0.28 ms, respectively. The amount of displaced charge $Q_{\infty 1}$ equals 0.39 nC. Comparison of the selected amperometric signal at −400 mV (circle) with the reconstructed current transient (red curve) is presented in Fig. 2a.

Here Fig. 2.

Agreement between the measured and the reconstructed current transients is rather good at times $t < t_{i2}$, (where $t_{i2} = 0.8\,\text{ms}$), and the root-mean-square deviation is about 0.03 μA (corresponding to 4.7 % of amplitude I_m). The numerically determined amplitude I_{m1} from the reconstructed current transient (using Eq. (26)) agrees very well with the experimental value (deviation amounts to 0.01 μA). At times $t < 0.15\,\text{ms}$, 3.8 % of the displaced charge $Q_{\infty 1}$ is not accounted for by the reaction kinetics model. The reconstructed current transient for the primary part of the

signal ends at times $t > 1.75\,\text{ms}$ (denoted as t_{d1} in Fig. 2a). The secondary part of the signal, appearing at times $t > t_{i2}$, could not be described by

the reaction kinetics model, although it contains a significant amount of displaced charge (half of the total displaced charge q_D). Therefore,

further analysis is performed within the time interval $t_{d1} - t_{i2}$ to obtain additional data relating to the secondary part of the signal, which is then

used for empirical fitting (shown by the blue curve in Fig. 2a). A new separated beginning of the secondary part of the signal (black triangle) is

obtained using a simple antilogarithmic subtraction of the reconstructed current transient (red curve) from the experimental data (circle). The

obtained additional data set relating to the secondary part of the signal consists of (black triangle) at times $t_{i2} < t < t_{d1}$ and (circle) at times

$t_{d1} < t < t_{d2}$. The corresponding data set is empirically fitted with two exponential functions of time (see blue curve in Fig. 2a). Determined

kinetic parameters include the time constants (τ_f and τ_s for the fast and slow components, respectively) and the amount of displaced charge

($Q_{\infty 2}$). The determined values of the time constants τ_f and τ_s are 0.42 ms and 1.04 ms, respectively. The amount of displaced charge, $Q_{\infty 2}$ of

0.38 nC is obtained. Fig. 2b shows a comparison of the selected amperometric signal at −400 mV (circle) with the overall best-fit curve of the

signal (solid black line) as a sum of (i) reconstructed current transient (red curve) of the primary part obtained from the model and (ii) empirical

fit of the secondary part of the signal (blue curve). Agreement between the measured and predicted data (using the sum of individual curves of

the primary part and the secondary part of the signal) is rather good. The value of root-mean-square deviation is about 0.02 μA (which

corresponds to 9.7 % of the maximum current value of the sum of individual curves). The total calculated displaced charge corresponds to

$Q_{tot} = Q_{\infty 1} + Q_{\infty 2}$. Deviation of the calculated displaced charge from experimental values is 0.01 nC, i.e. 1.3 %. Since the corresponding deviation is small, separate analysis of the primary part of the signal from that of the secondary part is therefore justified.

In general, the amperometric signal reflects the rate of the final state formation at the interface. The reaction kinetics model makes it possible to differentiate distinct states of the adhesion process (A, B, C, D) obtained from the time constants determined from the primary part of the signal and Eqs. (22), (23), (24) and (21), respectively. These states of the adhesion process can be associated with various features of the algal cell amperometric signal. Fig. 3a shows the four individual states coexisting from the beginning of the amperometric signal.

Here Fig. 3.

At the initial time $t = 0.05\,\mathrm{ms}$, the amount of state A is at its maximum value (A_0), while $B = C = D = 0$. The initial contact area of the cell can be expressed as $A_{c0} = V_0 / d_0$ and corresponds to 21.14 µm² (using the cell volume in the solution $V_0 = 108.67\,\mathrm{µm}^3$ and smaller axis a as the initial thickness of the cell $d_0 = 5.14\,\mathrm{µm}$). The amount of the initial state A, its corresponding volume V and contact area A_{c0} decrease exponentially with time. For the final state D, the volume can be calculated as $\Delta V = V_0 - V$ and the corresponding contact area A_{c1} can be obtained from the displaced charge at the interface (which is proportional to the amount of the final state D). The thickness of the organic layer can be calculated as $d_1 = \Delta V / A_{c1}$.

At the time point when the current reaches half of the current amplitude, the predominant state is the first intermediate state B, which could be associated with deformation. The intermediate state B is controlled by τ_0 and τ_1. The intact state A and the second intermediate state C, which could be associated with rupture, are present equally (about 25 %). The cell integrity probably remains, as supported by the fact that the extent of the final state D is below 3 % and the calculated thickness of the layer corresponds to 277 nm (see Fig. 3b). The presence of membrane proteins and cytoskeleton could help anchorage cell integrity [33], so collapse does not occur immediately like in the case of phospholipid vesicles. The cell contact area is one order of magnitude larger than the initial contact area of the cell at the interface.

At the time of current amplitude, the predominant state is the second intermediate state C, which could be associated with rupture and pore expansion. The intermediate state C is controlled by all three time constants (τ_0, τ_1 and τ_2), reaches its maximum at time t_{m} and becomes negligible at times $t > 1.75\,\mathrm{ms}$ matching with the end of the primary part of the signal. At the time of current amplitude, the intact state A almost disappears, while the first intermediate state B, associated with deformation, is present about 16 %. The final state D corresponds to almost 30 %. Since that the (i) cell spread contact area is two orders of magnitude larger than for intact cell and that (ii) the final layer is only about 35 nm thick, imply that the state C should be associated with cell rupture at the interface. These evidences support the interpretation that the major structural disruption of the cell membrane, collapse of cytoskeleton and leakage of intracellular material are likely to appear about the time of current amplitude. Electrochemical size detection limit in the de-aerated condition is ≥ 3 μm, therefore single organelle can not be detected, but the overall intracellular content. Evidence of the slower spreading at the interface is result of the mechanical resistance due to the intracellular organization that oppose to the spreading, and it is noticed as the current noise on the descending part of adhesion signal.

At the time of 0.8 ms, the secondary part of the signal starts, $A = B = 0$ and the predominant state is D corresponding to 86.5 %. The calculated thickness of the layer at the interface is about 12 nm. The cell contact area is 400 times larger than the initial contact area of the cell. The second intermediate state, C, drops to about 13 %. At times $t > 0.8\,\mathrm{ms}$, the value of V reduces to zero and consequently $\Delta V = V_0$. The corresponding total cell contact area is calculated as the sum of A_{c1} and A_{c2} and the film thickness as $d = V_0 / (A_{c1} + A_{c2})$. At the time of 4.45 ms the final film thickness reaches the value of 5.3 nm and the total cell contact area at the interface is almost three orders of magnitude larger than the initial contact area of the cell (see Fig. 3b). Fig. 4 shows illustration of attractive interactions between the algal cell and the positively charged electrode/aqueous electrolyte interface at the selected time points of adhesion signal.

Here Fig. 4.

Quantitative description of the temporal transformation of the cell at the interface is showed on Fig. 3b. Table 1 summarizes signal parameters and best-fit parameters of the reaction kinetics model and empirical fitting for selected amperometric signals of cells at various potentials.

Here Table 1.

Within the potential range of adhesion, the signal amplitude and signal direction depend on the surface charge of the electrode. Nearly twofold decrease of A_c values at the negatively charged electrode could be ascribed to the electrostatic repulsion between the negatively charged cells and negatively charged electrode, reflecting a slower adhesion and spreading process. Calculated values of displaced charges $Q_{\infty 1}$, $Q_{\infty 2}$ and the corresponding contact areas A_{c1}, A_{c2} obtained using the analysis of primary and secondary parts of the signal are comparable, and their sum agrees with the corresponding values q_D, A_c of the complete analyzed signal. No significant effect of potential on the values of time constants has been observed. The time constants obtained from the secondary part of the signal (τ_f and τ_s) are significantly lower than those of the primary part, which could be associated with the (i) attenuated effect of potential at the modified interface and (ii) stronger intermolecular interaction, reorganization of molecules in the film. The effect of potential on the double layer at the modified electrode differs from the free metal interface [34].

4.3. Visualization of plasma membrane vesicles

In order to obtain plasma membrane vesicles, a suspension of algal cells was exposed to hypotonic stress. Hypotonic conditions caused swelling of live cells, followed by subsequent cell rupture due to the osmotic shock and release of intracellular content. No significant structural changes are expected on the membrane, although different salt concentration might affect activity of enzymes and proteins on the cell membrane. On such a way is usually isolated membrane of the red blood cells. Light microscopy and AFM imaging were used to visualize the efficiency of

intracellular release. Under light microscopy, live cells were observed as green, elliptically shaped cells with two flexible flagella (Fig. 5a), while ghost plasma membrane vesicles (Fig. 5b) had an inflated balloon-like appearance and were larger than the original algal cell.

Here Fig. 5.

The plasma membrane vesicles were easily detected under fluorescence after staining with Nile red, as shown in Fig. 5c. Their diameter ranged from 5 to 20 μm. Vesicles larger than 25 μm were observed only rarely. Diameters of plasma membrane vesicles determined from AFM images (Fig. 6) were in line with the optical micrograph data.

Here Fig. 6.

The average thickness of the deflated part of vesicles was ~ 20 nm, suggesting that each membrane bilayer had a thickness of ~ 10 nm (Fig. 6a). The corresponding thickness is in line with the estimated cell envelope thickness of 9 nm under electron microscopy [11]. Such relatively high membrane thickness is likely to arise due the presence of water remains, other cell components trapped inside the membrane vesicles and due to the high glycoprotein content in the cell envelope. The *Dunaliella* cell "coat" appears to be made up of glycoproteins of ~150 kDa existing in the outer layer surrounding cells as proven by staining with cationic dyes [22]. In the high-resolution AFM image (Fig. 6b), proteins appear as

densely packed globules with a height of ~5-15 nm. According to the membrane proteome study of *D. salina* [35], these protein complexes may be surface coat proteins, lipid-metabolizing enzymes, ion transporters, GTP-binding proteins, heat shock proteins or other membrane proteins of unknown function.

4.4. Amperometric detection and adhesion kinetics of plasma membrane vesicles

Typical amperometric signal of the plasma membrane vesicle recorded at the potential of −400 mV is shown in Fig. 7 (circle).

Here Fig. 7.

Thus, for the selected amperometric signal of the plasma membrane vesicle with current amplitude of 1.08 μA, the signal duration is 0.60 ms, total displaced charge is 0.18 nC and the calculated area of the contact interface is 0.48×10^4 μm^2. We apply the reaction kinetics model of the three-step process to determine kinetic parameters of the adhesion from the amperometric signal shown in Fig. 7. The reconstructed current transient is obtained using the determined independent kinetic parameters (τ_0, τ_1, τ_2 and Q_∞) and Eq. (26). The values of time constants τ_0, τ_1 and τ_2, which refer to the attachment, deformation and spreading, are 0.02 ms, 0.03 ms, and 0.10 ms, respectively. The amount of displaced charge Q_∞ equals 0.39 nC. The best-fit curve (Fig. 7) shows that the agreement is rather good and the root-mean-square deviation is

about 0.04 µA (corresponding to 3.3 % of amplitude I_m). The numerically determined amplitude I_m from the reconstructed current transient (using Eq. (26)) agrees very well with the experimental value (deviation amounts to less than 0.01 µA). At times $t < 0.06\,\text{ms}$, 1.65 % of the displaced charge Q_∞ is not accounted for by the reaction kinetics model. Table 2 shows the time constants determined from the selected amperometric signals of plasma membrane vesicles at the positively and negatively charged interface using the reaction kinetics model of the three-step process.

Here Table 2.

From the comparison of amperometric signals of plasma membrane vesicles of the same current amplitude but recorded at potentials of −200 mV and −400 mV, it appears that the contact area is larger and the time constant (τ_2) is faster where maximum adhesion prevails, i.e. at potential of −400 mV. Comparing the results for the algal cell and its plasma mebrane vesicle (shown in Tables 1 and 2), it follows that (i) the isolated cell envelope contributes about one quarter to the cell contact area and (ii) the determined time constants referring to plasma membrane vesicle adhesion are faster than those for the algal cell. This difference can be ascribed to the contribution of the released intracellular content leading to attenuation of the potential at the interface. Further, the determined time constants of plasma membrane vesicle adhesion are of the same order of magnitude as for the DOPC vesicles, suggesting that the presence of glycoproteins on adhesion kinetics is not as significant. Fatty acids of chain lengths C16 and C18 are most abundant in the plasma membranes and microsomal membranes of *Dunaliella* [23]. We examined the temporal

transformation of a single plasma membrane vesicle in terms of the four states: initial A, intermediate B and C, and final D, referring to the intact state, deformed and ruptured states, and the organic film, respectively (see Fig. 8).

Here Fig. 8.

For a completely irreversible process, these states are reconstructed from the time constants of the selected current transient (shown in Fig. 7) and using Eqs. (22), (23), (24) and (21), respectively. At the initial time $t = 0.05\,\text{ms}$, the amount of state A is at its maximum value (A_0), while $B = C = D = 0$. Then, the amount of state A decreases exponentially with τ_0 and is essentially zero at times $t > 0.14\,\text{ms}$ (near t_{m} of current amplitude I_{m}). The first intermediate state B is controlled by τ_0 and τ_1, reaching its maximum value at the time of 0.07 ms (close to $t_{\text{m}}/2$ of current amplitude I_{m}) and becoming negligible at times $t > 0.25\,\text{ms}$. The second intermediate state C is controlled by all three time constants (τ_0, τ_1 and τ_2), reaches its maximum at time t_{m} and becomes negligible at times $t > 0.65\,\text{ms}$, when the final state of D is essentially completed 99.6 % ($D \approx A_0$).

5. CONCLUSION

The amperometric adhesion based detection of a single cell at the charged interface where conditions at the electrode mimic the electric field strength at the biological membrane is useful for electroporation based studies and for biomimetic research. We provide a kinetic interpretation of amperometric signals of an algal cell and its plasma membrane vesicle recorded under the near physiological conditions, where the accessed information improves our understanding of the sequence of steps involved in the mechanism of cell adhesion at the interface. We derive analytical solutions of the reaction kinetics model of the three-step adhesion process to decouple and identify temporal evolution of the four distinct states. The final state is expressed in the corresponding electrical equivalent in order to be used directly for amperometric measurements obtained with high time resolution. We demonstrate the validity and pertinence of the reaction kinetics model in the wide range of surface charge densities. Adhesion of intact cell is more complex process than adhesion of isolated plasma membrane vesicles at the interface. The difference in adhesion behavior between cell and its plasma membrane vesicle is associated with released intracellular content which significantly contributes to the contact area of *D. teriolecta* cell, which is missing in the case of rupture and spreading of vesicles, filled with aqueous electrolyte solution. Adhesion kinetics of the algal cell is slower than its plasma membrane vesicle. The model makes it possible to associate individual states with various features of the amperometric signal. At the time of current amplitude, the ruptured state predominates and the cell spread contact area is larger than the initial area of the free cell as well as the contact area of the plasma membrane vesicle Isolated cell envelope contributes about one quarter to the cell contact area as found at the potentail of -400 mV where interfacial tension of mercury electrode is close to its maximum value and the hydrophobic interaction is expected to prevail in cell adhesion. These results suggest that the major structural disruption of the cell membrane, collapse of cytoskeleton and leakage of intracellular material could appear close to the time of current amplitude. Further, kinetics of

the spreading of organic film at the charge interface to its maximal extent is considered as the rate determining step, which could be a consequence of the attenuated effect of potential at the modified interface, stronger intermolecular interactions and reorganization of molecules in the film. The isolated plasma membrane vesicle could mimic a biological membrane since it possesses a natural complex assembly of the proteins and the mixture of lipids, which is a step up from the commonly used model system such as phospholipid vesicle. The isolated plasma membrane vesicle shows a perspective for further development as the *in vitro* model to probe interfacial processes at the membrane.

Acknowledgments

References

[1] A. Nelson, Electrochemistry of mercury supported phospholipid monolayers and bilayers, Curr. Opin. Colloid Interface Sci. 15 (2010) 455.

[2] D. Bizzotto, Y. Yang, J.L. Shepherd, R. Stoodley, J. Agak, V. Stauffer, M. Lathuilliere, A.S. Akhtar. E. Chung, Electrochemical and spectroelectrochemical characterization of lipid organization in an electric field, J. Electroanal. Chem. 574 (2004) 167.

[3] R. Guidelli, G. Aloisi, L. Becucci, A. Dolfi, R. Monicelli, F.T. Buoninegni Bioelectrochemistry at metal | water interfaces, J Electroanal. Chem. 504 (2001) 1.

[4] S.H. Almaleck, F. Lairion, E.A. Disalvo, G.J. Gordillo, Lipid monolayers on Hg as a valid experimental model for lipid membranes under electrical fields, Chem. Phys. Lipids;139 (2006) 150.

[5] A.V. Brukhno, A. Akinshina, Z. Coldrick, A. Nelson, S. Auer, Phase phenomena in supported lipid films under varying electric potential, Soft Matter, 7 (2011) 1006.

[6] D. Hellberg, F. Scholz, F. Schauer, W. Weitschies, Bursting and spreading of liposomes on the surface of a static mercury drop electrode, Electrochem. Commun. 4 (2002) 305.

[7] D. Hellberg, F. Scholz, F. Schubert, M. Lovrić, D. Omanović, V.A. Hernandez, R. Thede, Kinetics of liposome adhesion on a mercury electrode, J. Phys. Chem. B, 109 (2005) 14715.

[8] V.A. Hernandez F. Scholz, Kinetics of Adhesion of DMPC Liposomes on a Mercury Electrode. Effect of Lamellarity, Phase Compositon and Presence of the Pore Forming Peptide Mastoparan X, Langmuir, 22 (2006) 10723.

[9] S. Kovač, R. Kraus, S. Geček, V. Žutić, Cell Suspension as a Model System for Electrochemical Analysis, Croat. Chem. Acta, 73 (2000) 279.

[10] V. Svetličić, N. Ivošević, S. Kovač, V. Žutić, Charge displacement and spreading of a cell: Amperometric signals of living cells, Langmuir, 16 (2000) 8217.

[11] V. Svetličić, N. Ivošević, S. Kovač, V. Žutić, Charge displacement by adhesion and spreading of a cell, Bioelectrochemistry, 53 (2001) 79-86.

[12] N. Ivošević DeNardis, V. Žutić, V. Svetličić, R. Frkanec, J. Tomašić: In Situ Amperometric Characterisation of Liposome Suspension with Concomitant Oxygen Reduction, Electroanal. 19 (2007) 2444.

[13] V. Žutić, V. Svetličić, A. Hozić Zimmermann, N. Ivošević DeNardis, R. Frkanec Comment on "Liposomes on a Mercury Electrode. Effect of Lamellarity, Phase Composition, Size and Curvature of Liposomes, and Presence of the Pore Forming Peptide Mastoparan X". Langmuir, 23 (2007) 8647.

[14] N. Ivošević DeNardis, V. Žutić, V. Svetličić, R. Frkanec, Amperometric Adhesion Signals of Lipsomes, Cells and Droplets, Chem. Biochem. Eng. Q, 23 (2009) 87.

[15] N. Ivošević DeNardis, V. Žutić, V. Svetličić, R. Frkanec, Adhesion signals of phospholipid vesicles at an electrified interface, J. Membrane Biol. 245 (2012) 573.

[16] P. Schön, J. Geerlings, N. Tas, E. Sarajlić, AFM Cantilever with in Situ Renewable Mercury Microelectrode, Anal. Chem. 85 (2013) 8937.

[17] V.A. Hernandez, J. Niesen, F. Harmisch, S. Bloch, A. Greinacher, H.K. Kroemer, C.A. Helm, F. Scholz, The adhesion and spreading of thrombocyte vesicles on electrode surfaces, Bioelectrochemistry, 74 (2008) 210.

[18] M. Hermes, F. Scholz, C. Härdtner, R. Walther, L. Schild, C. Wolke, U. Lendechal, Electrochemical Signals of Mitochondria. A New probe of Their Membrane Properties, Angewandte Chemie Int. Ed. 50 (2011) 6872.

[19] I. Ružić, N. Ivošević DeNardis, J. Pečar-Ilić, Kinetics of the liposome adhesion on a mercury electrode: testing of a mathematical model, Int. J. Electrochem. Sci. 4 (2009) 787.

[20] I. Ružić, J. Pečar-Ilić, N. Ivošević DeNardis, Mathematical model for kinetics of organic particle adhesion at an electrified interface, J. Electroanal. Chem. 642 (2010) 120.

[21] N. Ivošević DeNardis, I. Ružić, J. Pečar Ilić, S. El Shawish, P. Ziherl, Reaction kinetics and mechanicam models of liposome adhesion on charged interface, Bioelectrochemistry, 88 (2012) 48.

[22] M.A. Borowitzka, L.J. Borowitzka, Dunaliella, in: M.A: Borowitzka, L.J. Borowitzka (Eds.), Micro-algal biotechnology, Cambridge University Press, Cambridge, UK. 1988, p. 27.

[23] J. E. Ben-Amotz, W. Polle, D. V. Subba Rao, The Alga Dunaliella Biodiversity, Physiology, Genomics and Biotechnology, Science Publishers, New Hampshire, US, 2009.

[24] V. Žutić, V. Svetličić, N. Ivošević, A. Hozić, O. Pečar, Northern Adriatic mesocosm experiment Rovinj 2003: Dynamics of organic microparticles studied by the electrochemical technique, Period. Biolog. 106 (2004) 67.

[25] R.R. Guillard, Culture of phytoplankton for feeding marine invertebrates, in: W.L. Smith, M.H. Chanley (Eds.), Culture of Marine Invertebratae Animals, Plenum, New York, 1975, p. 22.

[26] G. Pletikapić, T. Mišić Radić, A. Hozić Zimmermann, V. Svetličić, M. Pfannkuchen, D. Marić, J. Godrijan, V. Žutić, AFM imaging of extracellular polymer release by marine diatom *Cylindrotheca closterium* (Ehrenberg) Reiman & J.C. Lewin, J. Mol. Recognit. 24 (2011) 436.

[27] V. Žutić, S. Kovač, V. Svetličić, Heterocoalescence between organic microdroplets and charged conductive interface, J. Electroanal. Chem. 349 (1993) 173.

[28] J.N. Israelachvili, Intermolecular forces & Surface forces, Academic Press Limited, New York, 1992.

[29] S. Orlowski, L.M. Mir, Cell electropermeabilization: a new tool for biochemical and pharmacological studies. Biochim. Biophys. Acta, 1154 (1993) 51.

[30] K. Olbrich, W. Rawicz, D. Needham, E. Evans, Effect of chain length and unsaturation on elasticity of lipid bilayers, Biophys. J. 79 (2000) 321.

[31] V. Svetličić, A. Hozić, Probing cell charge by scanning electrode potential. Electorphoresis, 23 (2002) 2080.

[32] V. G. Levich, Physicochemical Hydrodynamics, Prentice-Hall, London 1962.

[33] T. Odenthal, B. Smeets, P. Van Liedekerke, E. Tijskens, H. Van Oosterwyck, H. Ramon, Analysis of Initial Cell Spreading Using Mechanistic Contact Formulations for a Deformable Cell Model, Plos One, 9 (2013) e1003267.

[34] N. Ivošević, V. Žutić, Spreading and detachment of organic droplets at an electrified interface, Langmuir, 14 (1998) 231.

[35] A. Katz, P. Waridel, A. Shevchenko, U. Pick, Salt-induced changes in the plasma membrane proteome of the halotolerant alga Dunaliella salina as revealed by blue native gel electrophoresis and nano-LC-MS/MS analysis, Mol. Cell. Proteomics, 6 (2007) 1459.

Figure captions

Fig. 1. Adhesion signal of *D. tertiolecta* cell recorded in a deaerated cell suspension at the potential of −400 mV (surface charge density σ_{Hg} = 3.8 μC/cm^2) at the mercury electrode/0.1 M NaCl interface.

Fig. 2. Selected amperometric signal of the algal cell (○) recorded at the potential of −400 mV is presented in: (a) semilogarithmic plot and (b) linear-scale plot showing the reconstructed current transient (red curve) obtained from the model, antilogarithmic difference (▲) between the experimental data and reconstructed current transient, empirical fitting (blue curve) of the secondary part of the signal, and the overall best-fit curve of the signal (black line) as a sum of red and blue curves.

Fig. 3. Temporal evolution curves of: (a) the individual states describing the algal cell adhesion at the electrode, according to the reaction kinetics model of the three-step process. Normalized magnitudes of the initial intact state (A/A_0), intermediate deformed states (B/A_0, C/A_0), and the final organic layer (D/A_0), and (b) calculated cell contact area (red line) and calculated thickness of the organic layer (blue line).

Fig.4. Proposed mechanism of the cell adhesion and spreading at charged electrode/aqueous electrolyte interface at the selected time points of adhesion signal: a) initial time prior to the cell attachment, b) the time when the current reaches half of the current amplitude, c) the time of the current amplitude, and d) the final time of film formation.

Fig. 5. Optical micrographs of (a) the *D. tertiolecta* cell, (b) plasma membrane vesicle under phase contrast and (c) plasma membrane vesicle under fluorescence after staining with Nile red. The same scale bar of 10 μm applies to all images.

Fig. 6. AFM images of (a) the plasma membrane vesicle with (b) zoom showing details of membrane structure. Images are presented as height data with vertical scale of 150 nm (a) and topographic 3D view with vertical scale of 80 nm (b). Corresponding vertical profiles are shown along the indicating lines.

Fig. 7. Adhesion signal of the plasma membrane vesicle recorded at the potential of -400 mV (surface charge density $\sigma_{Hg} = 3.8$ μC/cm^2) at the mercury electrode/0.1 M NaCl interface ($\circ$) and the corresponding reconstructed current transient (solid line) obtained from the reaction kinetics model of the three-step process.

Fig. 8. Temporal evolution curves of the individual states describing the plasma membrane vesicle adhesion to the electrode, according to the reaction kinetics model of the three-step process. Normalized magnitudes of the initial intact state (A/A_0), intermediate deformed states (B/A_0, C/A_0), and final organic layer (D/A_0).

Table 1. Signal parameters and the best-fit parameters determined from the reaction kinetics model and empirical fitting for selected amperometric responses of the *D. tertiolecta* cells recorded at the positively and negatively charged electrodes. Accuracies in the evaluation of time constants are: $\tau_0 \pm 0.01$ ms, $\tau_1 \pm 0.02$ ms, $\tau_2 \pm 0.05$ ms, $\tau_f \pm 0.10$ ms and $\tau_s \pm 0.20$ ms.

Electrode conditions		Signal parameters					Reaction kinetics model					Empirical fitting			
E/mV	σ_{12}/μCcm^{-2}	I_{m1}/μA	I_{m2}/μA	t_d/ms	q_D/nC	A_c/10^4 μm^2	$Q_{\infty 1}$/nC	A_{c1}/10^4 μm^2	τ_0/ms	τ_1/ms	τ_2/ms	$Q_{\infty 2}$/nC	A_{c2}/10^4 μm^2	τ_f/ms	τ_s/ms
−200	11.50	0.98	0.13	2.05	0.54	0.47	0.39	0.34	0.05	0.06	0.22	0.14	0.12	0.28	0.51
−300	7.67	1.05	0.20	2.65	1.47	1.92	0.78	1.02	0.05	0.09	0.49	0.69	0.90	0.72	2.00
−400	3.80	0.73	0.20	4.45	0.78	2.05	0.39	1.03	0.06	0.10	0.28	0.38	1.00	0.42	1.04
−600	−2.44	−0.29	−0.05	1.50	−0.32	1.31	−0.13	0.53	0.04	0.08	0.25	−0.19	0.78	0.23	2.94
−700	−4.76	−0.59	−0.10	1.75	−0.51	1.09	−0.29	0.61	0.03	0.05	0.33	−0.23	0.48	0.44	1.19
−900	−8.26	−0.61	−0.11	1.85	−0.70	0.88	−0.35	0.42	0.04	0.09	0.33	−0.35	0.42	0.30	2.33

Table 2. Signal parameters and the best-fit parameters (τ_0, τ_1, and τ_2) for selected amperometric responses of the plasma membrane vesicles recorded at the positively and negatively charged electrodes. Accuracies in the evaluation of time constants are: $\tau_0 \pm 0.01$ ms, $\tau_1 \pm 0.01$ ms and $\tau_2 \pm 0.02$ ms.

Electrode potential	Surface charge density	Current amplitude	Signal duration	Displaced charge	Contact area	Time constants		
E/mV	σ_{12}/μCcm^{-2}	I_m/μA	t_d/ms	Q_∞/nC	A_c/$10^4\,\mu$m^2	τ_0/ms	τ_1/ms	τ_2/ms
−200	11.50	1.08	0.93	0.28	0.25	0.02	0.03	0.18
−400	3.80	1.08	0.60	0.18	0.48	0.02	0.03	0.10
−800	−6.50	−1.89	0.88	−0.50	0.77	0.03	0.04	0.16
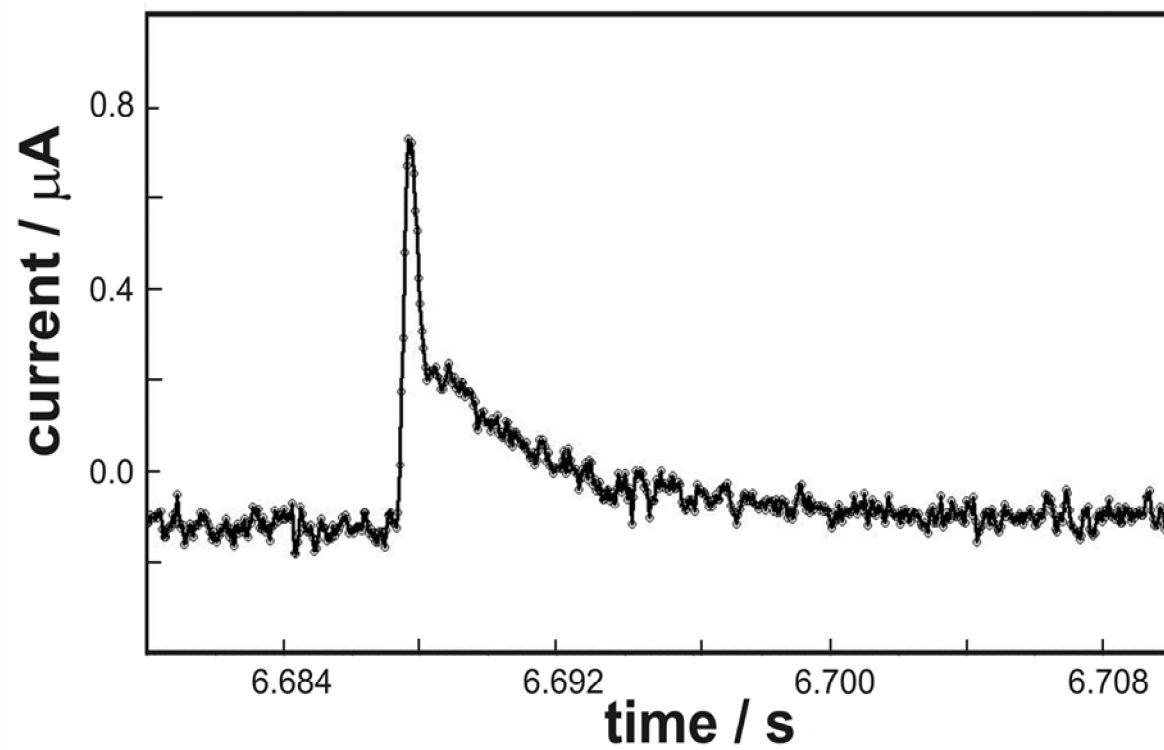
Fig_1_Ivosevic_DeNardis_et_al .
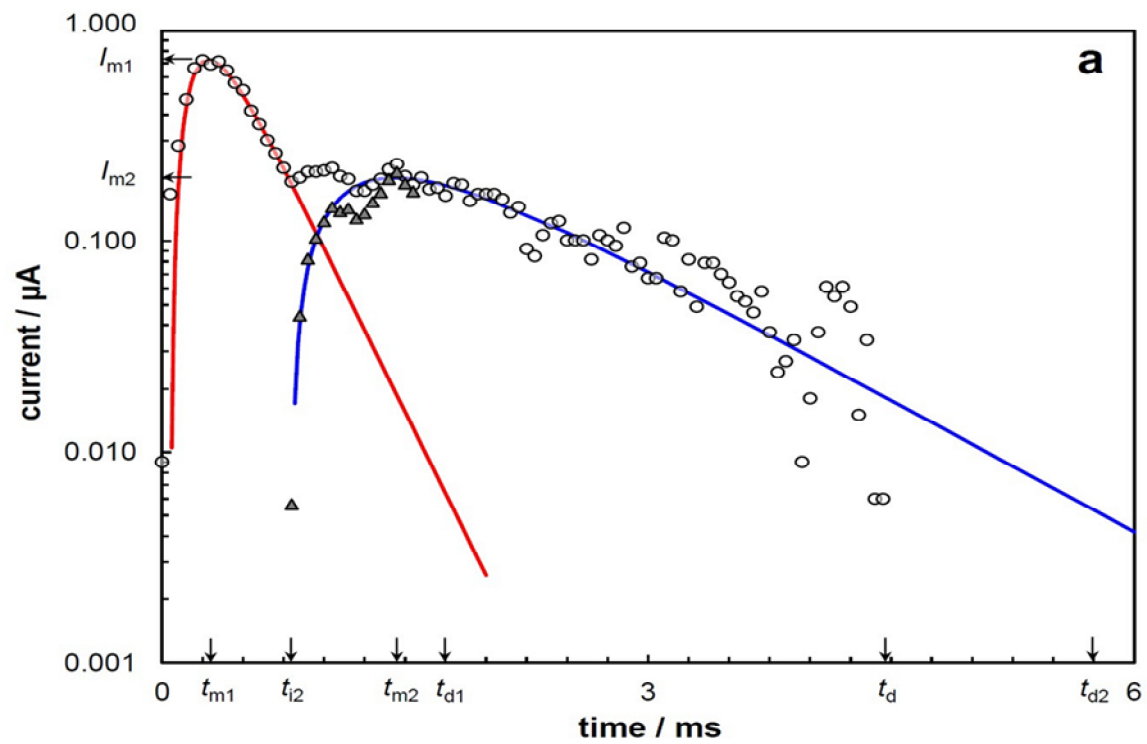
Fig_2a_Ivosevic_DeNardis_et_al .
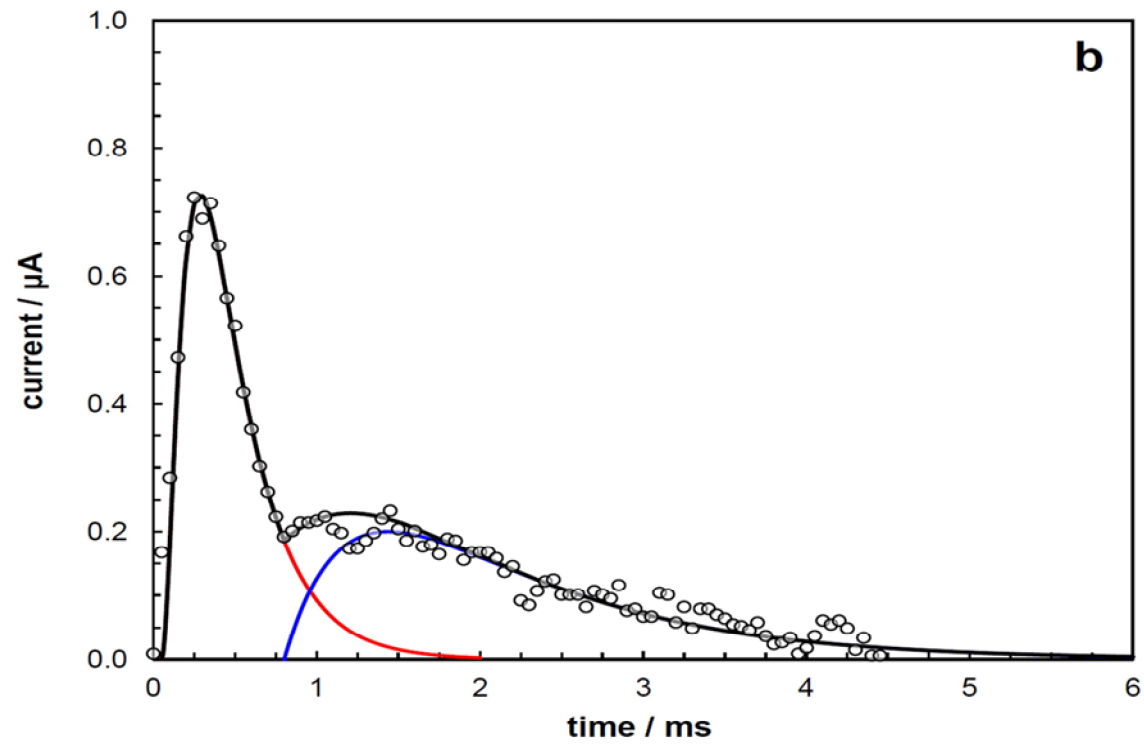
Fig_2b_Ivosevic_DeNardis_et_al .
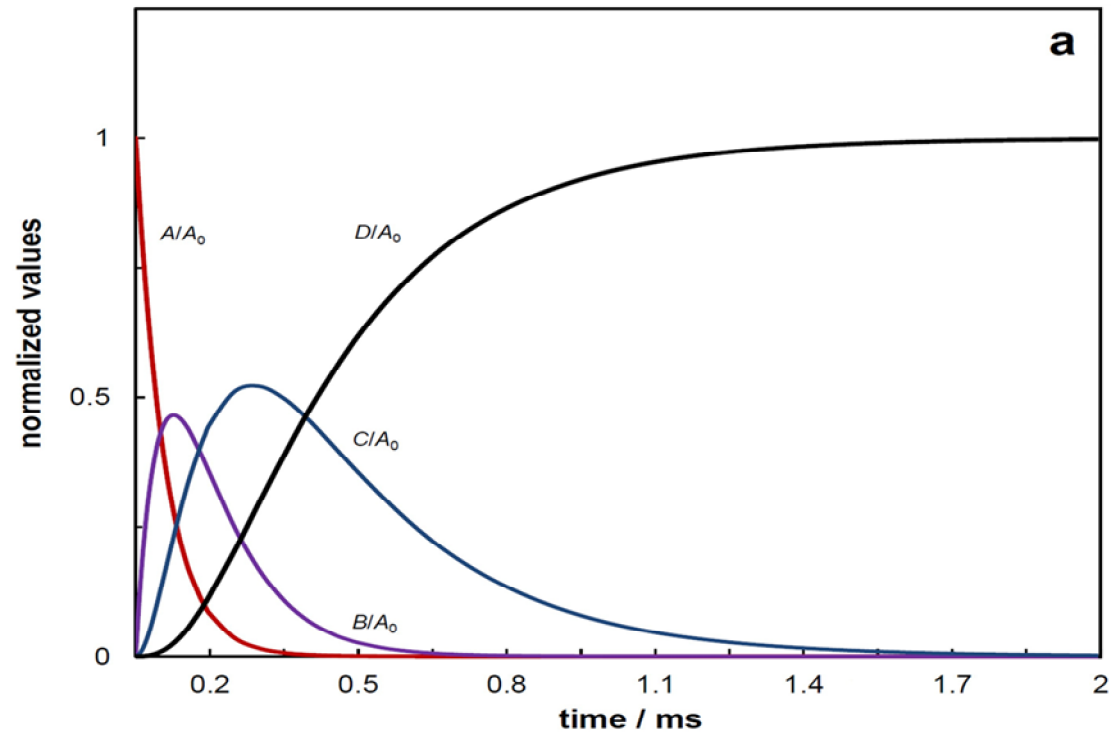
Fig_3a_Ivosevic_DeNardis_et_al .
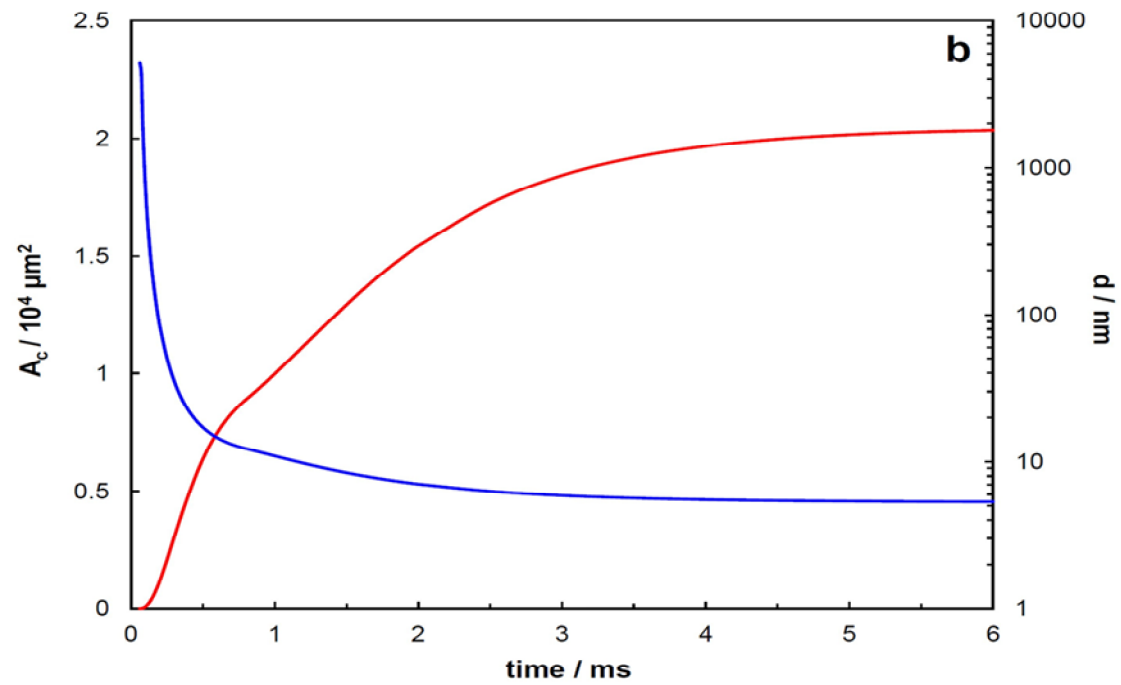
Fig_3b_Ivosevic_DeNardis_et_al .
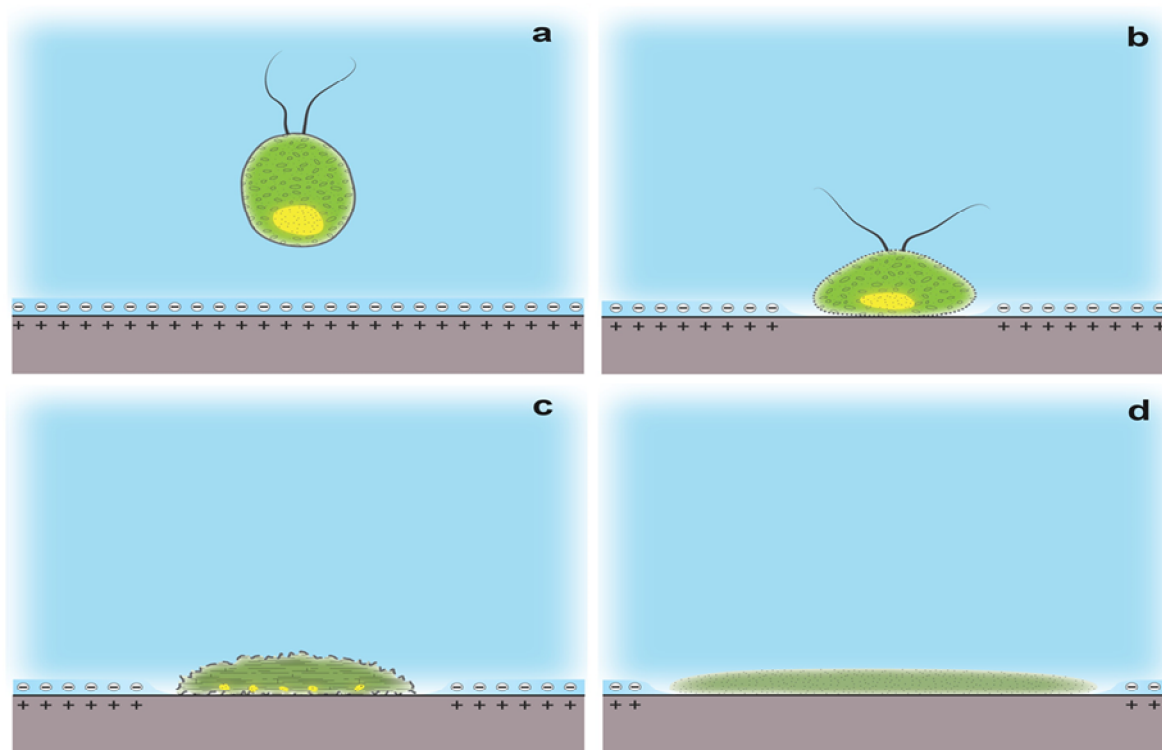
Fig_4_Ivosevic_DeNardis_et_al .
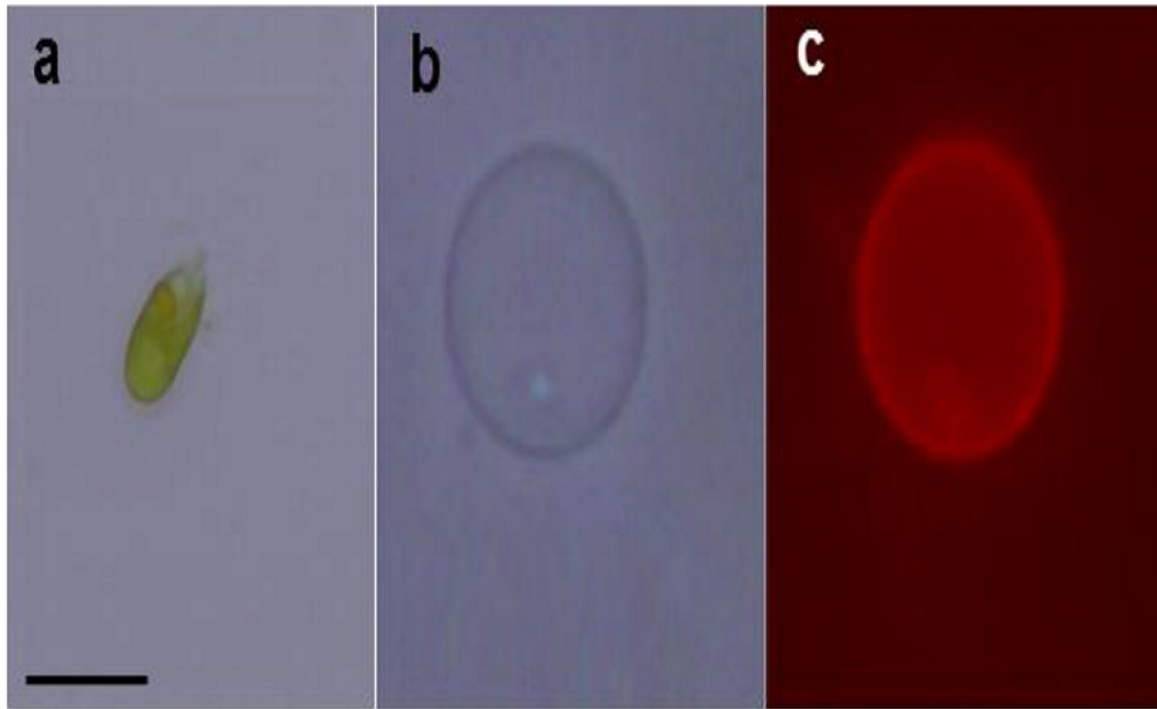
Fig_5_Ivosevic_DeNardis_et_al .
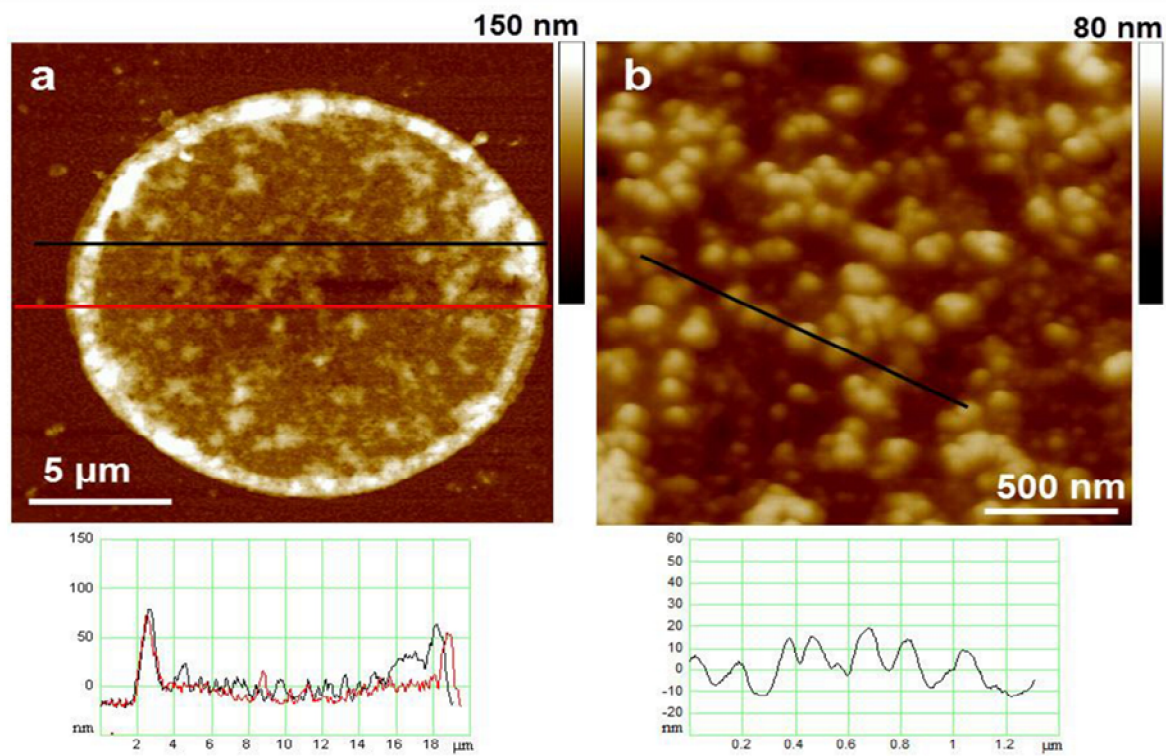
Fig_6_Ivosevic_DeNardis_et_al .
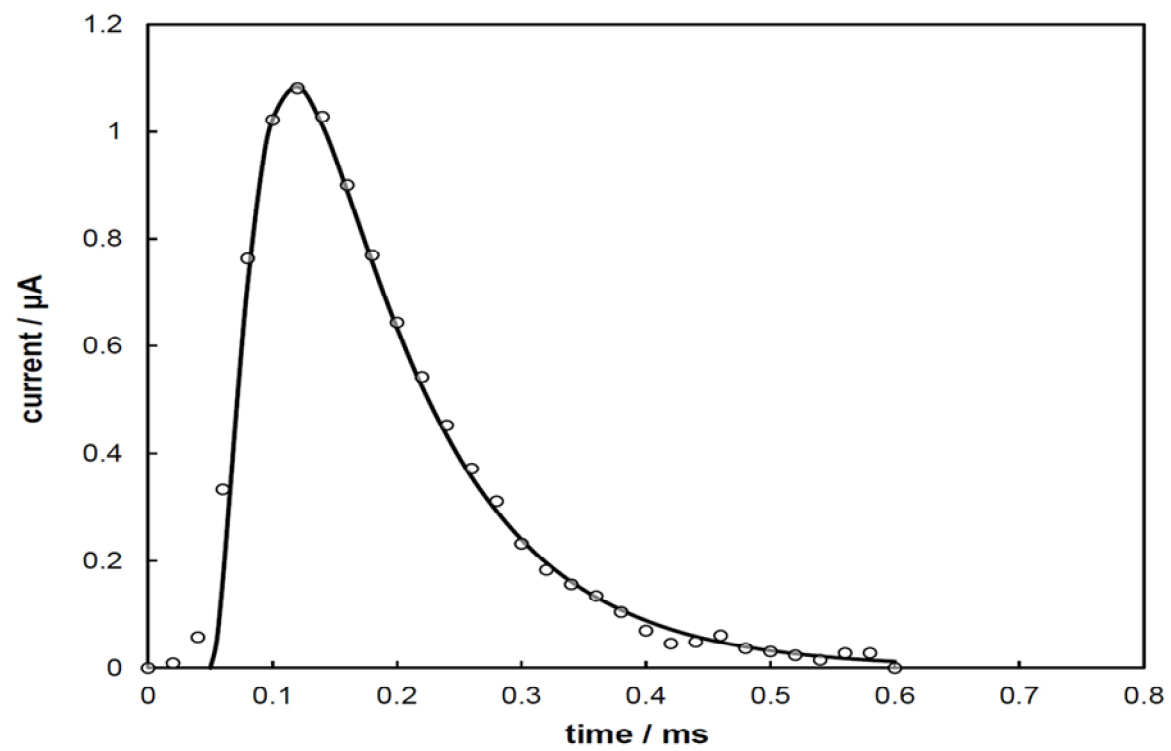
Fig_7_Ivosevic_DeNardis_et_al .

Fig_8_Ivosevic_DeNardis_et_al .